IEEE Access
Multidisciplinary ⋮ Rapid Review ⋮ Open Access Journal

Received 6 September 2023, accepted 15 October 2023, date of publication 20 October 2023, date of current version 30 October 2023.

Digital Object Identifier 10.1109/ACCESS.2023.3326367

RESEARCH ARTICLE

Improving Bearing Fault Identification by Using Novel Hybrid Involution-Convolution Feature Extraction With Adversarial Noise Injection in Conditional GANs

MUHAMMAD IRFAN[1], ZOHAIB MUSHTAQ[2], NABEEL AHMED KHAN[3], FAISAL ALTHOBIANI[4], SALIM NASAR FARAJ MURSAL[1], SAIFUR RAHMAN[1], MUAWIA ABDELKAFI MAGZOUB[5,6], (Member, IEEE), MUHAMMAD ARMGHAN LATIF[7], AND IMRAN KHAN YOUSUFZAI[2]

[1]Electrical Engineering Department, College of Engineering, Najran University, Najran 61441, Saudi Arabia
[2]Department of Electrical, Electronics and Computer Systems, College of Engineering and Technology, University of Sargodha, Sargodha 40100, Pakistan
[3]Department of Electrical Engineering, Riphah International University, Islamabad 46000, Pakistan
[4]Faculty of Maritime Studies, King Abdulaziz University, Jeddah 21589, Saudi Arabia
[5]Sudan Technological University, Omdurman 13315, Sudan
[6]National University, Khartoum 11111, Sudan
[7]Department of Computer and Information Systems, Cleveland State University, Cleveland, OH 44115, USA

Corresponding author: Muawia Abdelkafi Magzoub (muawia.magzoub@nu.edu.sd)

This work was supported by the Deanship of Scientific Research, Najran University, Saudi Arabia, through the Distinguished Research Funding Program under Grant NU/DRP/SERC/12/8.

ABSTRACT Bearing faults are critical in machinery; their early detection is vital to prevent costly breakdowns and ensure operational safety. This study presents a pioneering take on addressing the challenges of imbalanced datasets in bearing fault diagnosis. By mitigating issues such as mode collapse and vanishing gradients, our novel method employs Conditional Generative Adversarial Networks (CGANs) with spectral normalization and adaptive adversarial noise injection to generate high-quality bearing fault samples. This enhances generalization and robustness against noisy data, significantly improving the stability of CGAN training. To extract meaningful features from grayscale bearing fault images, we introduce a novel combination of involution and convolution feature extraction method named I-C FFN. This innovative feature extraction method captures both local and global information, making it capable of handling various types of features, including channel-agnostic, spatial-specific, spatial-agnostic, and channel-specific characteristics. Our proposed oversampling methodology helped enhance the performance of proposed classification scheme as well as of benchmark transfer learning models. Having accuracy values between 99.40% to 99.61% for 0 and 1 HP imbalanced dataset respectively, our models outperformed standard transfer learning methodologies. Furthermore, by the inclusion of our proposed Adaptive Adversarial Class-Conditional GAN (AAC-cGAN), the samples quality and the robustness to noise was significantly increased as demonstrated by the quantitative assessment through various Evaluation Metrics employed in this paper. Lastly, the performance of each combination of both the up-sampled and under-sampled methodologies were assessed through multiple metrics to determine the effectiveness of our proposed approach in addressing class imbalance in bearing fault diagnosis.

INDEX TERMS Conditional generative adversarial networks, involutional neural networks, convolutional neural networks, mode collapse, vanishing gradients, channel-agnostic, spatial-specific, feature extraction, deep learning.

The associate editor coordinating the review of this manuscript and approving it for publication was Yongming Li.

I. INTRODUCTION

An essential component of the manufacturing sector, ''Rotating machinery,'' is rapidly evolving in the direction of automation and intelligence amidst the backdrop of intelligent manufacturing. With the ever-expanding industrial needs, structures are becoming increasingly advanced and intricate [1], [8], [9], [10]. However, this progress also brings challenges. The bearing, a critical component in rotating machinery, often experiences wear and aging because of continuous high-paced operation during production. This wear and aging contribute to safety mishaps and can disrupt the entire production, leading to equipment damage and even injuries [2], [23], [24]. Consequently, manufacturing productivity can suffer. Thus, reliable system functioning depends on effective defect diagnostics.

The analysis of temperature, vibration, ultrasound, electrical discharge, and other variables is currently a part of bearing problem diagnosis technology [3], [5], [27], [28], [29]. The vibration signal is the one that is most frequently employed because data collection and processing are simple. Additionally, when a bearing's surface is partially damaged,periodic broadband pulse excitation signal will be produced, making it highly effective in analyzing the rolling bearing's vibrations. The essential steps of data-driven intelligent fault diagnostic approaches are the fault features extraction and classification of fault states. The existing approaches for extracting characteristics from vibration signals in rolling bearings encompass the combinations of time,frequency and time-frequency domain analyses. The time-frequency analysis among the three vibration signals is commonly employed, with methods like wavelet-transform(WT) [4], empirical mode decomposition(EMD) [5], [27], [28], [29], local mean decomposition(LMD) [6], and others being prevalent. These extracted characteristics serve the purpose of discerning fault conditions through basic machine learning techniques like random forests [7]. Nevertheless, these techniques are dependent on domain-specific knowledge, are unable to learn intricate features, and lack the necessary adaptability to handle situations involving substantial integration and intricate operational conditions.

The Deep Learning(DL) algorithms such as CNN learn features adaptively and extract features directly from raw vibration signals. – Eliminating the need for manual feature extraction with more efficient, significantly accurate and highly generalizable fault diagnosis. In this regard, researchers have used deep neural networks to evaluate the deterioration degree of rolling bearings based on the extracted fault feature information from vibration signals. Hence using a bottle-neck optimised convolutional neural network (MB-CNN) and multi-sensor data fusion, Wang et al. [1] suggested a unique fault recognition approach for rotating equipment. In order to prevent information loss, the created network executes the bottleneck layers with a larger input features. The innovative CNN achieves improved recognition and fast convergence. Similarly, Guo et al. [2] introduced an approach involving a multi-task CNN with integrated detail and employed dynamic training. This method allows for the concurrent execution of both fault diagnosis and localization tasks [3], [30], [31], [32], [33], [34].

CNNs possess the ability to extract intricate feature details without any manual labor from the high-dimensional input. If we can represent 1-D vibration signals from bearings in a matrix or spectral image format, effectively transforming these vibrational signals into two-dimensional representations, we can harness the feature extraction capabilities of CNNs to obtain more precise features. Huang et al. [3] introduced an innovative approach known as the ''deep decoupling CNN'' for a smart compound fault diagnosis. Initially, a 1-d deep CNN is used to learn distinctive characteristics from vibration signal. Subsequently, a multi-stack designed capsule is applied to separate the classifier, allowing for accurate identification and decoupling of faults that are composite. At the end, using the protocol routing algorithm and cost function the proposed model is optimized. Qiao et. al. [4] improved the CNN's sensitivity to fault characteristics by introducing an adaptable weight vector.

Where two dimensional transformations have large influenced the diagnosis of vibrational signals, Gray scale representation by reshaping the signals have been employed for feature extraction by deep learning methodologies. Adapting this methodology, Peng et. al. reshaped the fault signals into grayscale image, utilized this grayscale image for extracting fault features, and obtained an improved fault diagnosis outcome [5]. In the same manner, Wen et al. [6] transformed the vibrational signal into a two-dimensional image and fed a CNN for classification and diagnosis. This approach has garnered significant interest from numerous researches including the following paper.

Despite the automated feature extraction capabilities from 2-d images, some researchers have involved their endeavors in preprocessing the signals to amplify the hidden patterns for a much more robust and reliable diagnosis. One such strive by Li et al., [7] converted vibrational signals into an image by amalgamating vibrational acceleration with integrated displacement signal. Dual-stage Attention RNN (DA-RNN) and a convolutional attention module (CABM) into the training process. Ultimately, they classified the faults using a CNN embedded within the CBAM structure.

Considering a deficiency of fault classes, most datasets have a significant imbalance ratio of normal and fault classes. This imbalance presents a fundamental challenge in effectively training machine learning models. To address this issue, the usual methods for extracting features from imbalanced data is diversified into two main groups. First of which focuses on enhancing the effectiveness of cost-sensitive algorithms to enhance the accuracy of fault diagnosis when dealt with scarcity of samples. However, these cost-sensitive methods encounter two primary challenges: (1) fault classification costs are often problematic, and (2) performance evaluation of cost-sensitive algorithms are

often densely complex [11], [40], [41], [42], [43], [44], [45], [46], [47], [48].

The second category centers around data augmentation techniques, including up and under-sampling in order to address class imbalance. The basic approach used for over-sampling involves duplicating samples in underrepresented classes to balance the count. However, this has a potential to lead the model towards overfitting issues since no new knowledge is introduced. On the other side, reduces samples count in the majority classes to match the class with minority samples inevitably results in information loss [7], [8], [9], [10], [11], [40], [49], [50], [51], [53].

In the domain of fault diagnosis, the challenge of effectively extracting meaningful fault-related features from unbalanced single dimensional fault data to develop robust fault diagnosis methods has emerged as an intriguing and demanding problem. Reed et al. [8] used GAN to automatically generate real images from text descriptions. Radford et al. proposed the Deep cGAN, which generates high resolution images [9].

Tang et al. utilized a Wasserstein GAN (WGAN) to reduce discrepancies in the distribution of fault data [11]. Similarly, Wang et al. used GAN for the synthesis of new samples and performed fault diagnosis using superposition denoising auto-encoders (SDAE) [12]. Mao et al. used GAN to create minority class samples on a Fast-Fourier Transform (FFT) processed data [13]. Xuan et al. proposed a Multi-view GAN (MV-GAN) to automatically expand the image dataset [14]. Lee et al. harnessed GAN to generate empirical mode decomposition (EMD) energy spectrum data, achieving superior fault diagnosis results compared to traditional oversampling techniques [15]. Han et al. combined adversarial learning with CNN to enhance robustness [16]. Akhenia et al. applied multiple time-frequency feature extraction methods to create 2-d time spectrum images fault signals, subsequently using single image GAN (SinGAN) to generate data [17]. Tong et al. [18] employed an auxiliary GAN with spectral norm (ACGAN-SN) for bearing fault detection. Although GAN based oversampling methods have potentially alleviated the problems associated with the under-represented classes, their training process is difficult and challenging. Some of the complications associated with GAN Networks are i. Model Collapse due to small training sizes ii. Vanishing and Exploding gradients in deep networks. iii. Adversarial susceptibility, as small perturbation in input data can deceive the generator or discriminator resulting in faulty samples generation.

Keeping under consideration the above shortcomings, a novel conditional GAN based oversampling algorithm is proposed with the spectral normalization and adaptive adversarial noise injection approach to generate high quality bearing fault samples for the minority classes. Moreover, the proposed GAN based method effectively counters the mode collapse and vanishing gradients. Additionally, a novel combination of involution and convolution based feature extraction is used to capture the channel- agnostic, spatial specific and spatial agnostic and channel specific features from the faulty bearings. This holistic approach provides a well-rounded understanding of the data, yielding both local and global insights crucial for accurate and reliable rolling bearing diagnosis. The contributions of this paper are enlisted below:

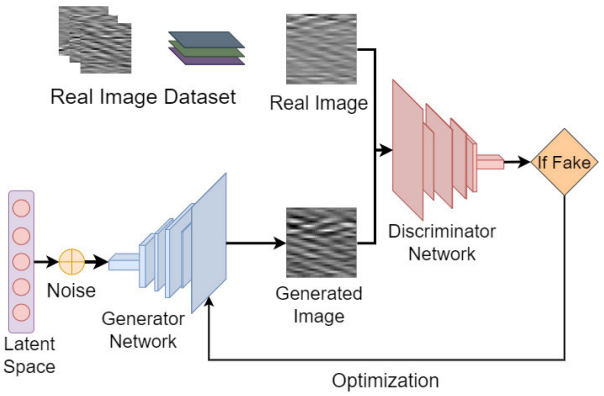

FIGURE 1. Generative Adversarial Network (GAN) architecture.

1) A novel GAN based up-sampling method is proposed to generate quality bearing fault samples with a stabilized training using spectral normalization and an adaptive adversarial noise injection mechanism for improved generalization and enhanced robustness to noisy data.
2) A novel involution and convolution based feature extraction method is proposed to capture the local and global details of bearing faults gray-scaled images. The use of channel-agnostic and spatial specific involution kernel compliments the single channeled nature of the transformed data and provide attention maps for each spatial window.

The remaining paper portion is structured as follow: The second section provides a brief Background of the techniques used. The Third Section explains the Methodology while the Fourth Section is for the discussion of results. The last section Concludes the paper.

II. MATERIALS AND METHODOLOGY

A. GENERATIVE ADVERSARIAL NETWORK–GAN

An adversarial trained generator (G) and discriminator (D) neural network pair make up a Generative Adversarial network (GAN) [11], [12], a deep learning framework that generates realistic data samples. The generator G in the mathematical implementation of a GAN aims to learn mapping from noise to data samples that mimic D., where is taken from a straightforward distribution like Gaussian noise, is how it is denoted. The discriminator is simultaneously attempting to discriminate between genuine samples produced by and fraudulent ones created by. This adversarial process is formalized as a min-max game in which seeks to reduce and seeks to increase the likelihood that correctly labels its generated samples as false. Mathematically, this can

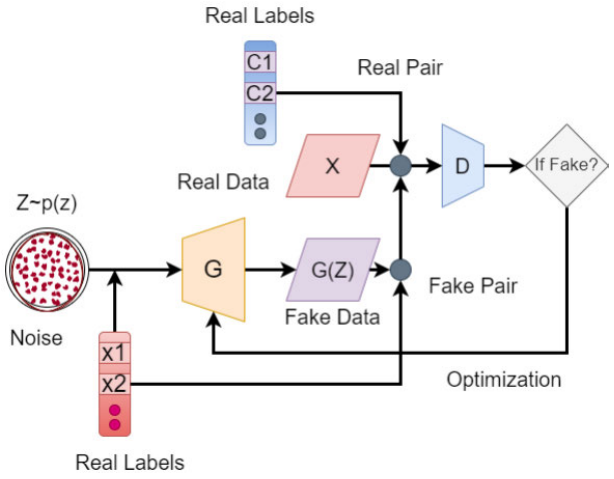

FIGURE 2. Class conditional- GAN architecture.

be expressed as:

$$min_G, max_D E_{x\sim D}[log(D(x))] + E_{z\sim Noise}[log(1 - D(G(z)))] \quad (1)$$

In this case, the probability reflects the probability assigns to a real sample, while the probability represents the probability assigns to a created sample. The GAN training procedure is carried out repeatedly until generates samples that are identical to real data, rendering incapable of efficiently discriminating between them. Due to this equilibrium, the generator generates data whose distribution roughly mimics that of the initial dataset.

B. CLASS CONDITIONAL GAN–cGAN

Conditional Generative Adversarial Networks (cGANs) [11], [12], [13], [14] are an extension of traditional GANs designed for controlled image generation. Unlike standard GANs, cGANs take additional information, often class labels, as input during the training process. In a cGAN, the generator takes both random noise and a conditional label as inputs. The discriminator also receives the same label along with real or generated images.

$$\min_G \max_D \mathbb{E}_{x\sim p_{\text{data}}(x|y)}[\log D(x \mid y)] + \mathbb{E}_{z\sim p_z(z),y}[\log(1 - D(G(z \mid y) \mid y))] \quad (2)$$

where,

x = real image
$G(z \mid y)$ = generates a fake image with label y
$D(x \mid y)$ = The probability value of Discriminator that the input image real.

The objective function for cGANs combines the standard GAN objective with an additional conditioning term, Mathematically given as:

Bearing fault diagnosis is a critical task in various industrial domains, ensuring the operational reliability and safety of machinery. Accurate detection and classification of bearing faults are paramount to prevent costly breakdowns and minimize downtime. However, this endeavor is marked by a fundamental challenge: the scarcity of labeled fault data compared to healthy data samples, leading to an imbalanced dataset problem. As Generative Adversarial Networks (GANs) are prone to challenges such as sub-optimal sample generation, mode collapse, and gradient disappearance. Researchers have proposed various techniques to address these issues and enhance GAN performance. Additionally, deep learning models, including GANs, are susceptible to adversarial attacks due to their dependence on learned parameters. Adversarial attacks can cause misclassification, which can prove critical in applications like machinery monitoring, where misclassifications can result in safety risks. Most current research studies in the domain of bearing fault diagnosis haven't addressed these shortcomings for GAN related oversampling in a single setting, according to our knowledge.

Therefore, in response to this challenge, we introduce AAC-cGAN (Adaptive Adversarial Class - Conditional GAN), a novel generative framework tailored for the synthesis of bearing fault signals. AAC-cGAN effectively counters two crucial issues that have a substantial effect on the training and the generation of quality samples i.e., Spectral Stability and Adversarial Robustness. Spectral Stability ensures the model's smooth training and resistance to exploding and vanishing gradients, whereas the adversarial robustness equips the model to generate good quality samples while also dealing with discrete noise patterns that can interfere with classification. Below is a thorough explanation of the proposed oversampling method.

C. ADAPTIVE ADVERSARIAL CLASS CONDITIONAL GAN–(AAC-cGAN)

In a Conditional GAN (cGAN), the generator (G) and the respective discriminator (D) are conditioned on particular class labels. These class labels help us generate data that belongs to specific classes. The generator takes random noise Z and a class label y as input and generates samples $G(z, y)$. The proposed method Adaptive Adversarial Class Conditional GAN (AAC-cGAN), makes use of the foundational principles of cGAN, and adds to the knowledge by introducing a spectral normalization layer in the discriminator section and an adaptive noise generation network that controls the amount of adversarial noise injected within the generator as part of the robust training regimen. The adaptive noise generation network is trained separately on the generator loss accumulated by a baseline GAN network, it is then integrated into the AAC-cGAN training loop to generate the controlling parameters (α and β) by passing GAN Loss as input to trained Adaptive Noise Generation Network (ANG). The general implementation of the method is given within Figure 3. While further elaboration of the ANG network and the related concepts is given in succeeding sections.

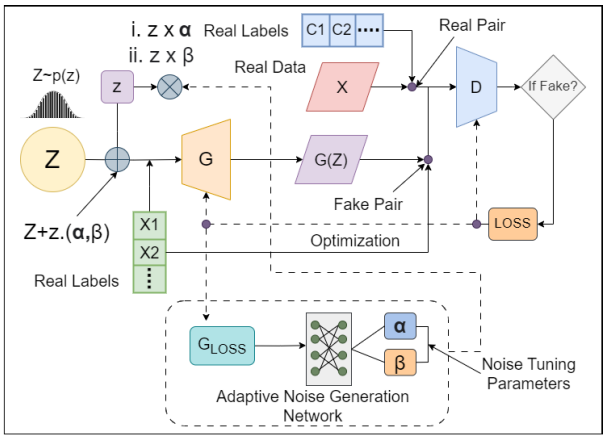

FIGURE 3. Proposed AAC-cGAN architecture.

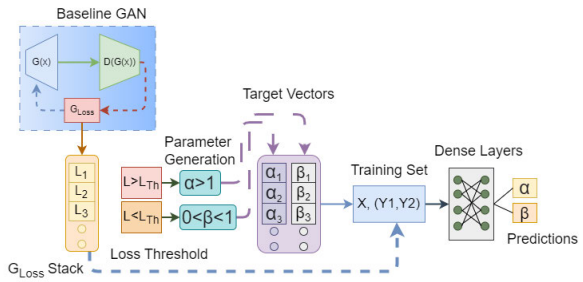

FIGURE 4. Adaptive Noise Generation (ANG) network.

1) ADAPTIVE NOISE GENERATION NETWORK

The Adaptive Noise Generation (ANG) network proposed in this paper is designed to dynamically generate noise adjustment factors (α and β) based on the current value of the Generator Loss (G_{Loss}) during training. This technique enables AAC-cGAN to adaptively control the magnitude and type of adversarial noise introduced into the generator's input.

The ANG network consists of feed-forward NN with one or more dense layers. G_{Loss} is given as input and the model outputs the noise adjustment factors α and β. The G_{Loss} fed to ANG network is extracted each epoch from a baseline GAN trained on respective experimental data. A suitable threshold L_{Th} value is manually selected from the acquired G_{Loss} stack as depicted in Figure 4.

Based on the threshold, α and β target variables are generated using a conditioning that will later be used as a guiding mechanism for adaptive noise generation. The generation of α and β target variables are done using the following constraints:

$$G_{Loss} \geq L_{Th} \tag{3}$$

Increase the magnitude of adversarial noise.

$$Z_{\text{noisy}} = Z + z \cdot \alpha \mid \alpha > 1 \tag{4}$$

If,

$$G_{Loss} \leq L_{Th} \tag{5}$$

Decrease the magnitude to avoid over-regularization.

$$Z_{\text{noisy}} = Z + n \cdot \beta \mid 0 < \beta < 1 \tag{6}$$

After the generation of target labels and creating a training set, the corresponding features and target variables are fed to the feed-forward network given as under.

$$InputLayer \Rightarrow [G_{Loss}] \tag{7}$$

$$\text{Hidden Layer} \Rightarrow H_i = \sigma(W_i \cdot H_{i-1} + b_i) \tag{8}$$

$$\text{Output Layer}_{\alpha} \Rightarrow \sigma(W_{\alpha} * H_n + b_{\alpha}) \tag{9}$$

$$\text{Output Layer}_{\beta} \Rightarrow \sigma(W_{\beta} * H_n + b_{\beta}) \tag{10}$$

where,

G_{Loss}	= Generator Loss
i	= layer number
σ	= activation function (e.g., ReLU or Sigmoid)
W_i and b_i	= weight and bias for i^{th} layer
W_α, W_β, b_α, and b_β	are weight matrices and bias for the output layer

2) NOISE INJECTION INTO GENERATOR

We introduced controlled noise Z_{noisy} generated by the ANG-Network into generator's input.

$$H_o = Dense(Z_{noisy}) \tag{11}$$

Here,

H_o = output of the dense layer that takes the noisy input Z_{noisy}.

The generator processes the noisy input Z_{noisy} and produces a synthetic sample X_{fake} such that,

$$X_{fake} = f\theta G(Z_{noisy}, y) \tag{12}$$

X_{fake}	= generated synthetic sample.
$f\theta G$	= generator function.
Z_{noisy}	= noisy input.
y	= class label.

3) DISCRIMINATION

The discriminator evaluates the authenticity of X_{fake} by considering both the class label y and the presence of added noise. Its output D_{output} indicates the prediction of the input resembling a real sample.

$$D_{output} = f\theta D(X_{fake}, y) \tag{13}$$

where,

D_{output}	= discriminator's output.
$f\theta D$	= discriminator function.
X_{fake}	= generated synthetic sample.
y	= class label.

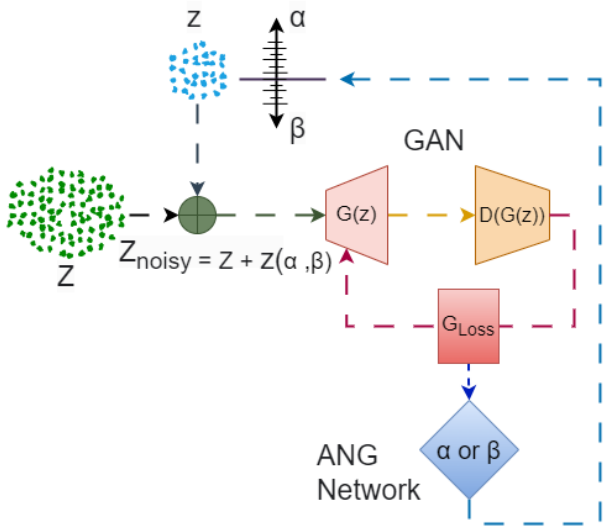

FIGURE 5. Illustration of adversarial noise injection.

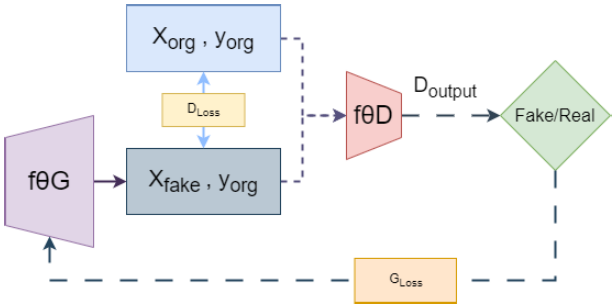

FIGURE 6. Working of discriminator.

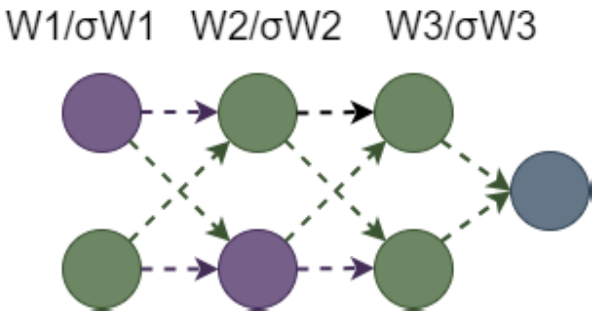

FIGURE 7. Spectral normalization.

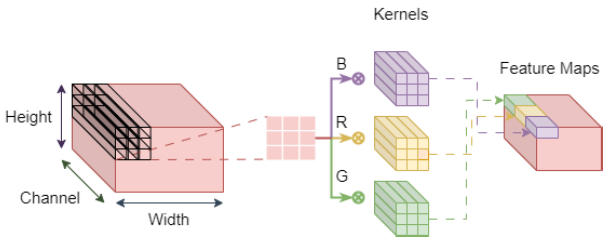

FIGURE 8. CNN architecture.

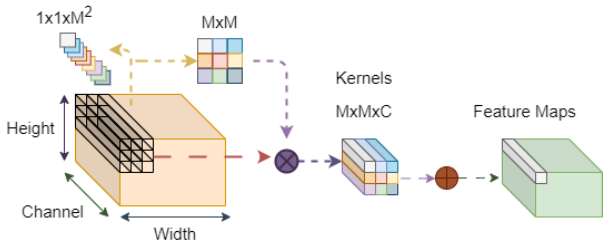

FIGURE 9. i-NN architecture.

4) SPECTRAL NORMALIZATION

Spectral normalization is a technique used to constrain the Lipschitz constant of neural networks in order to enhance training stability. In AAC-cGAN, weight matrices W of discriminator are stabilized by applying spectral normalization, further ensuring that the Lipschitz constant of these networks does not exceed a specified threshold.

$$\tilde{W} = \frac{\sigma(W)}{W} \tag{14}$$

here,

$\tilde{W}$ = spectrally normalized weight matrix.
W = original weight matrix.
$\sigma(W)$ = largest singular value of W.

D. CONVOLUTIONAL NEURAL NETWORK–(CNN)

In traditional convolutional neural networks (CNNs), convolution is performed on data tensor D of shape (n, C, H, W), where n represents number of samples, C is the number of channels, and H and W are the spatial dimensions. Convolutional filters (also known as kernels) are applied to the input data while each filter has weights shared across all spatial positions. Mathematically, the output K for a single filter can be represented as:

$$C_i = \sum_{j=1}^{N} (F \cdot K_i)_j \tag{15}$$

where,

C_i = Output features of i^{th} convolutional layer.
N = Filter count
F = Feature map obtained from involutions.
K_i = i^{th} convolutional kernel.

E. INVOLUTIONAL NEURAL NETWORK–(i-NN)

Involutional Neural Networks (i-NNs) [19] are a novel neural network architecture for computer vision tasks. They introduce "involution," an operation that adaptively combines input values using learned parameters associated with specific positions in the input, enhancing spatial sensitivity. i-NNs challenge traditional convolutional design principles, achieving improved performance in tasks like image classification and object detection while often reducing computational costs. This innovative approach bridges

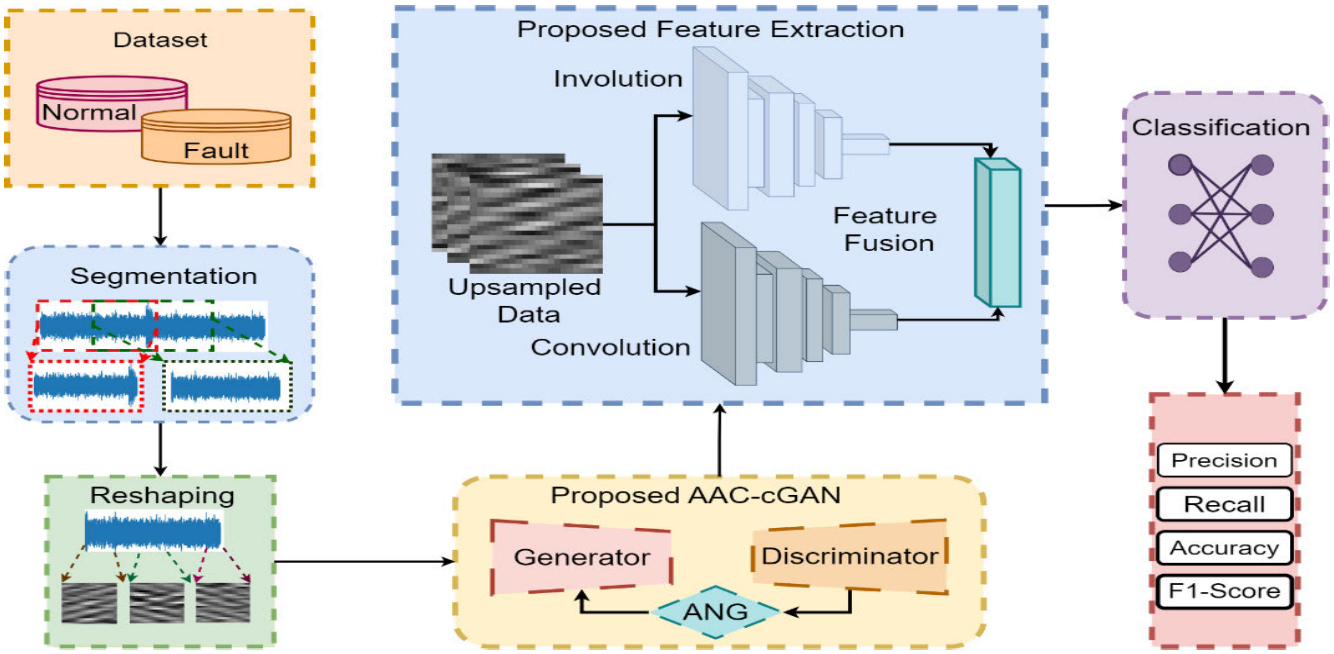

FIGURE 10. Block diagram of proposed bearing fault classification scheme.

convolution and self-attention mechanisms, making it a promising tool for efficient and effective deep learning in visual recognition. Involution aims to invert the design principles of convolution, making it more location-sensitive and channel-agnostic.

In an involutional layer, instead of using shared weights for all spatial positions, distinct weights are used for different spatial positions. Mathematically, the output P for a single position (i, j) can be represented as:

$$p_{\text{val}} = x_i + m - \left\lfloor \frac{K_{\text{size}}}{2} \right\rfloor, j + n - \left\lfloor \frac{K_{\text{size}}}{2} \right\rfloor, c \tag{16}$$

$$P_{i,j} = \sum_{m=1}^{K} \sum_{n=1}^{K} K_{m,n} \cdot p_{\text{val}} \tag{17}$$

$P_{i,j}$ is the output at position (i,j) in the feature map for channel c. $K_{m,n}$ is the input value at position m. p_{val} is pixel values from the input image at shifted positions based on kernel size for channel c. K is the size of the filter.

F. PROPOSED FEATURE EXTRACTION METHOD

Involutions is a new concept that hasn't been much explored. Involutions offer a new take towards feature extraction, by effectively inverting the working of convolutional neural networks, Involutional networks provide an attention based mechanism through a spatially-specific and channel-agnostic approach. Involutions capture non-local dependencies and global context, enabling the understanding of intricate relationships within data. Convolutions, on the other hand, excel at learning hierarchical and abstract features, essential for recognizing patterns and objects within localized regions.

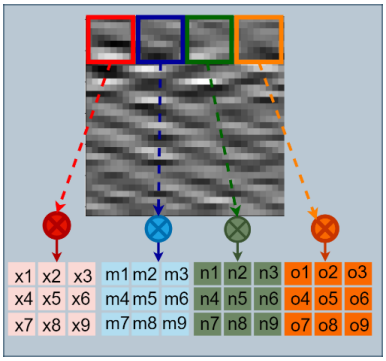

FIGURE 11. Channel agnostic and spatial specific feature extraction by involution kernel.

When used in synergy within neural network architectures, involutions and convolutions create powerful feature extraction pipelines. Their combination allows networks to capture both local and global information, resulting in representations that are not only informative but also discriminative. Herein, we propose such synergy of the aforementioned feature extraction techniques named Involution-Convolution Feature Fusion Network (I-C FFN) for feature extraction of bearing fault gray-scaled 2-dimensional representations, that will not only benefit from a channel-agnostic approach and a spatially inclined involution network but also a global context extracting CNN network, all in a computationally inexpensive and reliable manner.

1) INVOLUTION BASED FEATURE EXTRACTION

For each element $x(i, j)$ in the input matrix X, our proposed involution network compute a weighted sum of the

TABLE 1. Layer description for proposed I-C FNN feature extraction methodology.

Layer	Description	Channel	Group Number	Kernel Size	Stride	# of Layers
Input	Input layer	3	-	-	-	1
Involution 1	Involution layer	3	3	5	1	2
Activation	ReLU	3	-	-	-	3
MaxPooling2D	MaxPooling2D	3	-	-	-	4
Involution 2	Involution layer	3	3	3	1	5
Activation	ReLU	3	-	-	-	6
Dropout	Dropout = 0.2	3	-	-	-	7
Involution 5	Involution layer	3	3	3	1	8
Involution 6	Involution layer	3	3	5	1	9
Involution 7	Involution layer	3	1	5	1	10
MaxPooling2D	MaxPooling2D	3	-	-	-	11
Conv2D	filters = 36, kernel = (3, 5), padding = 'same'	36	-	(3, 5)	-	12
Conv2D	filters = 36, kernel = (3, 7), padding = 'same'	36	-	(3, 7)	-	13
MaxPooling2D	MaxPooling2D	36	-	-	-	14
Conv2D	filters = 36, size = (1, 5), padding = 'same'	36	-	(1, 5)	-	15
Conv2D	filters = 36, size = (3, 5), padding = 'same'	36	-	(3, 5)	-	16
MaxPooling2D	MaxPooling2D	36	-	-	-	17
Conv2D	filters = 36, size = (3, 7), padding = 'same'	36	-	(3, 7)	-	18
Conv2D	filters = 36, size = (3, 9), padding = 'same'	36	-	(3, 9)	-	19
Concatenation	Concatenation	-	-	-	-	20
Activation	ReLU	-	-	-	-	21
Global Avg. Pool	-	-	-	-	-	22
Dense	Dense layer with units = 99, activation = "relu"	99	-	-	-	23
Dense	Dense layer with units = 23, activation = "relu"	23	-	-	-	24
Dense	Dense layer with units = 14, activation = "softmax"	14	-	-	-	25
Output	Output layer	-	-	-	-	26

surrounding elements, allowing for the incorporation of local information. The involution kernels move around each spatial location $(xi + k, j + l)$ with different weights, capturing the local context and extracting the most informative region by utilizing self-attention. While doing so the same weights in a kernel are applied to each channel within the receptive field. Resulting in a low computation matrix operation and a channel agnostic approach. This method proves effective in dealing with single channeled images, where color channels hold very little information like the bearing fault gray-scaled images used in this study. This operation is given as:

$$y(i, j) = \sum_{k=1}^{K} w_k \cdot x_{i+k,j+l} \tag{18}$$

$y(i, j)$ is the output at position (i, j) and K is the kernel size, which defines the size of the local receptive field.w_k represents the weights applied to the neighboring elements while $x_{i+k,j+l}$ represents the neighboring elements around (i, j).

Involutions are performed across the entire input matrix, resulting in a feature map F that retains important local patterns. The architecture begins with input images of size 32 × 32 with 3 channels, typical for color images. It employs a series of Involution Layers, each with distinct configurations. The Involution Layers capture spatial dependencies effectively. The first Involution Layer ("inv_1") applies a 5 × 5 kernel with a group number of 3, reducing the spatial dimensions slightly. Next is the ReLU activation and max-pool to down-sample the feature maps. Subsequent Involution Layers ("inv_2", "inv_5", "inv_6", and "inv_7") follow similar patterns, further refining spatial relationships and features. These layers utilize different kernel sizes, striving to capture patterns at various scales. Finally, a max-pool layer is applied to down-size the feature map.

2) CONVOLUTION BASED FEATURE EXTRACTION

The convolution section of our proposed feature extraction pipeline is based on multi-layered feature extraction. With multiple kernels that slide over the feature map F, computing

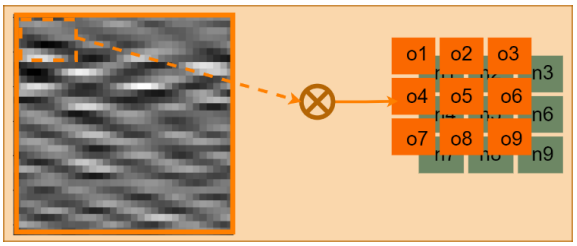

FIGURE 12. Channel specific and spatial agnostic feature extraction by convolution kernel.

a weighted sum of local patches, global details are extracted. While the channel specific approach, applied computationally expensive matrix operation of varying weighted kernel with each channel to acquire color details. These global details were made available to the classification network for fault diagnosis. Mathematically, a convolution operation can be represented as:

$$C_i = \sum_{j=1}^{N} (F \cdot K_i)_j \tag{19}$$

where:

C_i = output feature map of the i^{th} convolutional layer.
N = number of filters.

The Convolution Layers in proposed I-C FFN architecture are fundamental for extracting global features from input images. These layers are meticulously configured with specific parameters to effectively capture channel specific and global aspects of the data. In the first Convolution Layer, a filter size of 3 ×5 is employed with 'same' padding, while the second layer uses a 3 ×7 filter with the same padding option. Both of these layers consist of 36 filters. A 2 ×2 max-pooling operation follows to down-sample the feature maps. The third Convolution Layer utilizes a 1 ×5 filter with 'same' padding, and the fourth layer employs a 3 ×5 filter with the same padding. These layers also consist of 36 filters each. Another 2 ×2 max-pooling layer follows these Convolution Layers. Additionally, the fifth and sixth Convolution Layers apply filters with sizes 3 ×7 and 3 ×9, both using 'same' padding and consisting of 36 filters each. These layers collectively contribute to a rich feature representation, crucial for the architecture's success in tasks such as multi-class classification and feature extraction from bearing fault signals.

3) FEATURE CONCATENATION

The feature fusion of convolution and involution layers allows the network to benefit from the unique advantages of each operation. As discussed above, the Involution captures spatial dependencies effectively and operates in a channel-agnostic manner, rendering it adept at recognizing complex patterns. On the other hand, Convolution is proficient at detecting basic features and structures in a global feature extraction approach. The features of both these layers were concatenated

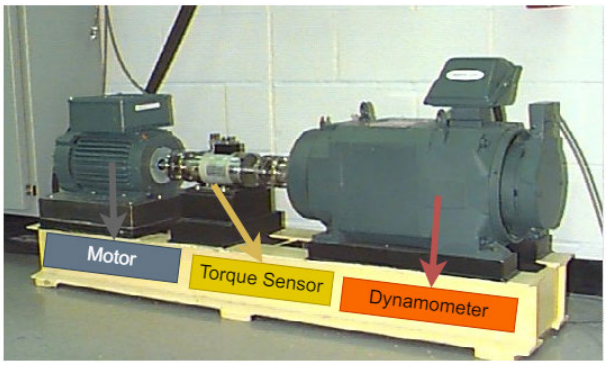

FIGURE 13. Bearing fault acquisition setup.

to form a final feature vector, arming the model with holistic understanding of the input data, combining fine-grained details captured by Involution with broader context revealed by Convolution. This synergy enhanced the network's ability to extract discriminative features, making it a powerful tool for our required gray-scaled images.

The feature concatenation operation between the output of the Involution Layers (denoted as Y_{inv}) and the output of Convolutional Layers (denoted as Y_{conv}) can be represented mathematically as follows: Y_{inv} is of shape $H \times W \times C_{inv}$, where C_{inv} is the number of channels after the Involution Layer. Y_{conv} is of shape $H \times W \times C_{conv}$, where C_{conv} is the number of channels after the Convolutional Layer. The feature concatenation operation can be represented as:

$$Y_{\text{concat}} = \text{concat}(Y_{\text{inv}}, Y_{\text{conv}}) \tag{20}$$

where,

Y_{concat} = Concatenated feature map.
$Concat$ = Concatenation two feature maps along the channel dimension.

III. EXPERIMENTAL RESULTS

A. CWRU DATASET

The dataset used herein for empirical analysis is CWRU (Case-Western-Reserve University)rolling bearing dataset[31], a vastly used, recognized, and open-source dataset that serves as a benchmark in diagnosing bearing faults. CWRU is developed by the Center-For-Intelligent Maintenance Systems (IMS) at Case Western Reserve University, aims to provide researchers and practitioners with standardized dataset for effective evaluation and comparison of different fault diagnosis methods and algorithms.

The dataset was meticulously designed to simulate the real-world conditions of various bearing faults and incorporating signals associated with various fault types. It comprises vibration signals recorded using an accelerometer from four sets of rolling element bearings operating under diverse conditions, including normal and faulty scenarios. These bearings are deep groove type, specifically (6205/6203- 2RS JEM SKF). The Data extraction procedure involved a set of equipment, including a 2-horsepower motor, transducer,

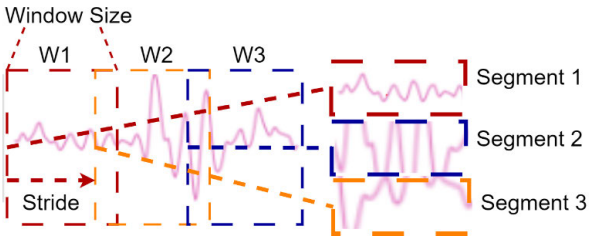

FIGURE 14. Segmentation of signals.

and dynamometer, as illustrated in Figure 13 [52]. Different fault conditions were intentionally introduced to individual bearings, encompassing inner-race, outer-race, and ball-faults, as well as combinations thereof. In order to ensure realism and consistency, fault sizes were precisely controlled. The Faults were integrated at specific points in order to create fault sizes on bearing races and balls. The respective faults were introduced in the test bearings supporting the motor shaft using electro-discharge machining, with fault diameters ranging from 7 mils to 40 mils, where 1 inch equals 1000 mils. NTN and SKF(Bearing Types), were employed for different fault diameters, such as 28 and 40 mils for NTN bearings and 7, 14, and 21 mils for SKF bearings.

Accelerometers were affixed to the housing with magnetic bases to extract vibrational data. The data acquisition process also involved rotating the bearings at distinct speeds and conditions to capture signals details under varying operating conditions. Acceleration data was collected from the sensors which were placed at different locations. These positions include, perpendicular to fan and drive ends of the motor housing. The acquisition sampling rates were 12,000 samples per second and 48,000 samples per second for drive end bearing faults. Additionally, the torque transducer was used to extract speed and horsepower data. For comprehensive analysis, the response to outer raceway faults, faults were strategically positioned relative to the load zones. For both the fan and drive-end bearings, the impact quantification was conducted via a series of experiments involving the placement of outer raceway faults at different orientations.

B. EVALUATION

In the following study, the fault dataset for 48K samples was used. The fault diameter of 0.007, 0.014 and 0.021 inches were also taken at zero and one horse-power (0HP,1HP) for classification. Additionally, the normal baseline data was merged with the prior mentioned data to be classified alongside. The empirical procedures to evaluate the proposed model's efficiency were based on and 14 classes respectively. The raw-signals were segmented using a window size of 1024 with a stride size of 500.

The stride of 500 ensured that the correlation and patterns between successive segments are captured. The segments are then reshaped into the corresponding 2-dimensional gray scale image representation allowing us to harness the spatial feature extraction capabilities of convolutional and attention based feature extraction. This further allowed the

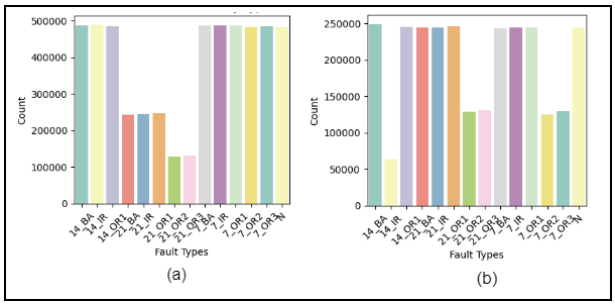

FIGURE 15. Class distribution of imbalance fault data (a) N-L condition (b) S-L condition.

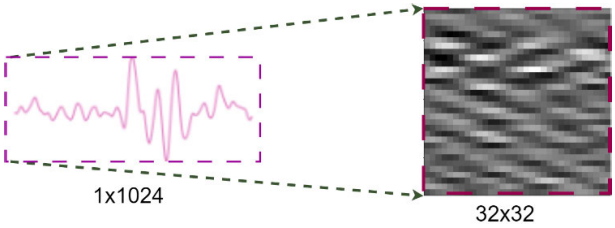

FIGURE 16. 1-D time domain signal conversion to 2-D gray scaled images.

feature extraction without any explicit noise reduction or preprocessing because of the deep learning based feature extraction framework and simplicity in synthetic sample generation.

AAC-cGAN was implemented on the imbalanced dataset as seen in the figure, for effective oversampling. The dataset with N-L and S-L conditions contain 13 fault classes and a healthy class in each, as shown in the figure. The numbers before the underscore represent the fault diameters in inches while the OR, IR and BA represent the Outer Race, Inner Race and Ball Faults. The number with the OR class represents the orientation at which the faults were induced. The class imbalance can be clearly seen in the figure which we will mitigate using the proposed up-sampling methodology.

The gray-scale image dataset of dimensions 32×32 was subjected to a baseline GAN model for generative loss extraction by training for 300 epochs and then a secondary model ANG was trained on the acquired generative loss. The ANG network took generative loss as input and outputs adjustment parameters α and β. This feature of ANG network is leveraged in the AAC-cGAN network for tuning the value of injected noise by placing it between the Generator Loss and the injected noise generator. The entire AAC-cGAN model was trained for 100 epochs and evaluated on multiple metrics providing a quantitative assessment of the generated samples epoch by epoch as shown in Figure.

To ensure the quality of samples generated and the performance of our proposed AAC-cGAN model with a baseline cGAN, we employed multiple evaluation metrics used for quantitative assessment of the model. Although these metrics provide a general overview of the model's performance, there is no one-fits all values contrary to our

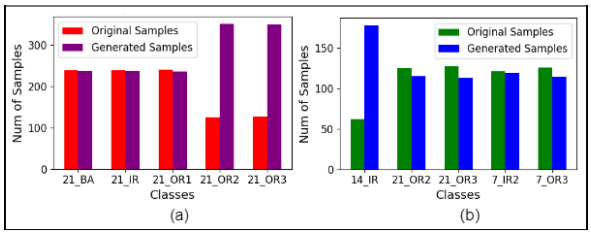

FIGURE 17. Upsampling ratio of imbalanced classes (a) N-L condition (b) S-L condition.

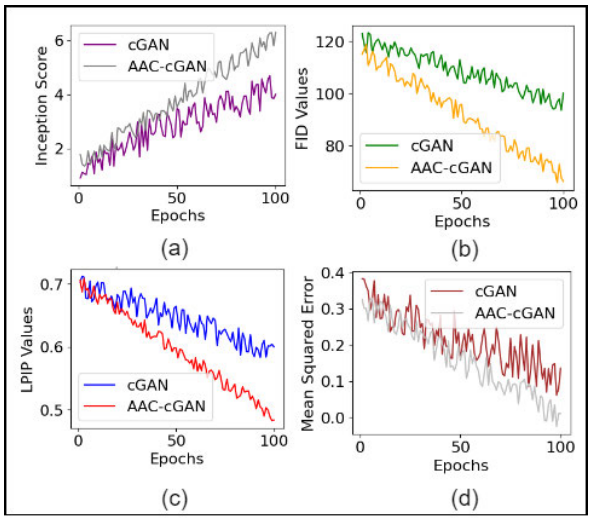

FIGURE 18. Evaluation metrics for cGAN and AAC-cGAN (a) Inception score (b) Frechet inception distance (c) Learned perceptual image patch similarity (d) Mean squared error.

general classification models. The figure above provides an epoch wise assessment for the duration of 100 epochs. As we approached the Nash equilibrium during the training regimen, the generated samples were quantitatively compared to the respective original counterparts. The first of the which is the inception score I-S, the I-S metric uses a pre-trained Inception-Net algorithm to evaluate the sample in terms of their quality and diversity. The above training curve for 100 epochs showed an increasing value for both c-GAN and our proposed AAC-cGAN model. As higher values of inception scores depict a better image quality, the baseline cGAN landed at a 3.8 while our proposed model had a score of 6.1. Similarly, the second curve shows the Frechet Inception Distance (FID), this distance metric quantifies the similarity of samples in the feature space. A lower distance value is a sign of a stable sample generation which can be seen in the training curve. The FID value for the cGAN stood at 103 while the proposed method landed at 67.5. Similarly, another metric Learned Perceptual Similarity Patch (LPIP) metric is employed to evaluate the perceptual similarity levels. This metric holds great significance as it quantifies the similarity levels similar to human vision. The curve in the figure shows a stable fall towards an improved LPIP score for both the cGAN and AAC-cGAN. The last metric is the MSE which although is not a direct evaluation of the

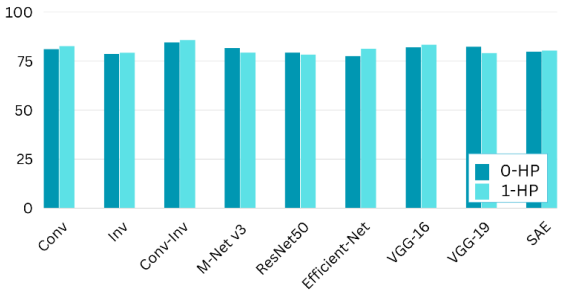

FIGURE 19. Accuracy assessment for imbalanced dataset on custom and pre-trained networks.

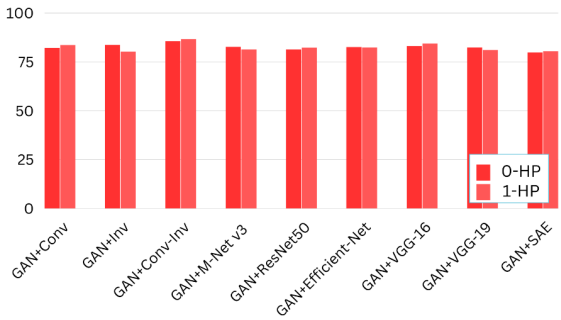

FIGURE 20. Accuracy assessment for cGAN based upsampling on custom and pre-trained networks.

generative models, but provides an insight into the fidelity of the model. Being a full reference metric, the lower values are considered better. Hence the above metrics allude to a quantitative estimation of improved image generation by our proposed model. It can be seen that the proposed technique clearly outpaces the baseline cGAN network in all quality metrics. Proving the effectiveness of our model in handling the under-study problem.

In order to get a more comprehensive evaluation of our proposed scheme, the experimental procedures were procured on different combinations. The initial experimentations were performed on the dataset with no-load (N-L) and single load (S-L) conditions (0-HP and 1-HP) without any oversampling. In this regard, multiple pre-trained and custom networks were used. The accuracy values were not optimal, as the highest accuracy reached at 85.94% and 83.46% by the proposed I-C FFN network for the respective 0 and 1 HP load conditions. The pre-trained networks that reached the highest accuracy for N-L condition was VGG-19 with 82.33% and for S-L condition VGG-16 reached 81.75%. The acquired accuracy values for under-sampled experimentations are given in Table 3. The above results indicate the significant room for improvement on the baseline results. The lower accuracy owes to the fact that the pre-trained networks haven't been acclimatized to the respective domain resulting in a mediocre result. With the additional under-sampled representations some classes are difficult to classify because of the sample scarcity. Hence rendering the overall performance compromised. Furthermore, these baseline results effectively guide to a better understanding of the models suitable for the task.

TABLE 2. Comparison of our model with existing works.

Ref.	Method	Description	Dataset	Accuracy	Drawbacks
[20]	Signals To Spectrograms	Lite Convolutional Neural Network	CWRU	99.65%	Limited to spectral features
[21]	Signal to Wavelet	Vibration data with Noise super-imposition for classification	CWRU	92.5%	Requires complex simulations
[22]	Signal To Wavelet	SuperResolution GAN and Wavelet Convolutional Capsule Network	CWRU	99.92%	Sensitive to noisy data
[23]	Signal To Gray Scale Images	Novel Deep Residual Network	CWRU	99.98%	Limited to grayscale information
[24]	Signal To Scattergram	Ensemble Of Multiple Imaging Methods and Res-Net50	CWRU	99.89%	Requires integration of various methods
Our Study	Signal to Gray Scale Images	Novel AAC-cGAN for oversampling, Involution-Convolution Hybrid feature extraction	CWRU	99.61%(1-HP) 99.40%(0-HP)	Computational resource requirements

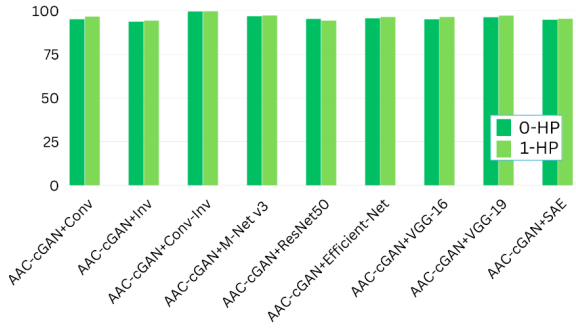

FIGURE 21. Accuracy assessment for proposed AAC-cGAN based upsampling on custom and pre-trained networks.

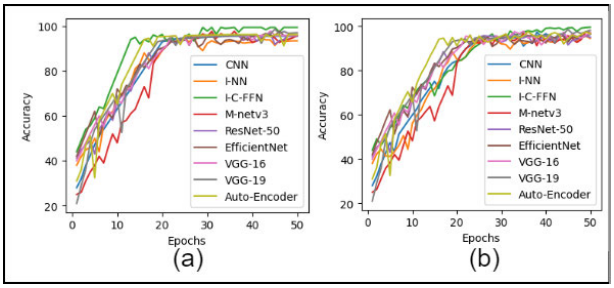

FIGURE 22. Accuracy curves of proposed and pre-trained models (a) Accuracy value for N-L condition (b) Accuracy value for S-L condition.

Following which, multiple experimentations were performed with the oversampled dataset using proposed and already established techniques for a thorough evaluation.

The results after the oversampling using baseline GAN provided some improvements albeit not quite significant, but sufficient to nudge us in the right direction. The highest accuracy attained was 86.09% on S-L and 85.13% on NL condition by our proposed classification model in this evaluation test, getting an increase of approx. 1.5% for N-L and 1% for S-L as shown in the Table 4. The rest of the pre-trained and custom models lagged just a little behind yet got an improvement in their results against the under-sampled outcomes. The reason our proposed model aced both the evaluation was its global and local feature extraction capability. Making it adept to tasks involving both channel agnostic and specific data. Although the GAN based oversampling was procured, however the sample quality was not optimal making feature extraction difficult and consequently affecting the potential of reaching higher. This drawback was overcome by introducing some changes within the baseline GAN's architecture to cater to the needs of our under-study problem.

After the evaluation through the baseline GAN, AAC-cGAN based oversampling is employed to integrate essential improvements by analyzing the shortcomings of baseline GAN. The training curves were more stable and the different quantitative assessments provided a much more comprehensive overview. The highest accuracy values achieved after applying AAC-cGAN on the synthetically oversampled

TABLE 3. Evaluation of models without oversampling.

Models	Accuracy	Recall	Precision	F1-Score	K. Stats	Matt. Corr.
Conv	79.56	79.28	79.84	79.56	80.24	80.24
	80.24	80.04	80.44	80.24	80.64	80.64
Inv	77.26	77.04	77.48	77.26	78.84	78.84
	78.84	78.64	79.04	78.84	79.44	79.44
I-C FFN	83.46	83.22	83.69	83.46	85.94	85.94
	85.94	85.74	86.14	85.94	87.34	87.34
M-Net	80.97	80.77	81.17	80.97	78.99	78.99
	78.99	78.79	79.19	78.99	79.79	79.79
ResNet	79.56	79.34	79.78	79.56	77.94	77.94
	77.94	77.74	78.14	77.94	79.14	79.14
Eff.Net	76.24	76.04	76.44	76.24	79.87	79.87
	79.87	79.67	80.07	79.87	81.27	81.27
VGG-16	80.94	80.75	81.13	80.94	81.75	81.75
	81.75	81.55	81.95	81.75	82.55	82.55
VGG-19	82.33	82.11	82.55	82.33	80.06	80.06
	80.06	79.86	80.26	80.06	80.86	80.86
SAE	80.13	79.94	80.32	80.13	80.95	80.95
	80.95	80.75	81.15	80.95	81.75	81.75

dataset as per the Table 5 were 99.40% and 99.61% for the proposed method I-C FFN shortly followed by VGG-19 with the accuracy value of 97.72% and 98.26% for N-L and S-L conditions. The rest of the transfer learning models also achieved a significant increase after the proposed oversampling methodology.

C. COMPARISON WITH EXISTING WORKS

The comparison of our method with the existing works reveal some scintillating insights into the advantages of our proposed method. The combination of cGAN and Adversarial Noise not only increases the quantity of training data but also bolsters the model's resilience against noisy data and potential adversarial attacks, a significant facet that is often overlooked in other studies such as [55], [56], and [57] where

TABLE 4. Evaluation of models with cGAN based over-sampling.

Models	Accuracy	Recall	Precision	F1-Score	K. Stats	Matt. Corr.
Conv.	81.04	80.83	81.25	81.04	82.76	82.76
	82.76	82.56	83.06	82.76	83.56	83.56
Inv.	82.47	82.25	82.69	82.47	79.84	79.84
	79.84	79.64	80.04	79.84	80.44	80.44
I-C FFN	85.13	84.95	85.31	85.13	86.09	86.09
	86.09	85.90	86.28	86.09	87.18	87.18
M-Net	81.07	80.91	81.23	81.07	80.21	80.21
	80.21	80.01	80.41	80.21	80.81	80.81
ResNet	80.44	80.28	80.60	80.44	80.97	80.97
	80.97	80.77	81.17	80.97	81.77	81.77
Eff.Net	81.36	81.20	81.52	81.36	81.18	81.18
	81.18	81.00	81.38	81.18	81.78	81.78
VGG-16	83.92	83.75	84.09	83.92	84.77	84.77
	84.77	84.57	85.07	84.77	85.57	85.57
VGG-19	83.97	83.79	84.15	83.97	82.91	82.91
	82.91	82.71	83.11	82.91	83.71	83.71
SAE	81.87	81.71	82.03	81.87	82.09	82.09
	82.09	81.91	82.29	82.09	82.89	82.89

TABLE 5. Evaluation of models with AAC-cGAN for N-L and S-L.

Models	Accuracy	Recall	Precision	F1-Score	K. Stats	Matt. Corr.
Conv.	95.51	94.27	94.26	95.11	95.45	95.44
	96.55	95.12	95.33	96.15	96.21	96.33
Inv.	93.53	93.45	92.29	93.12	93.56	93.54
	94.57	94.25	94.29	94.24	94.17	94.17
I-C FFN	99.40	99.34	99.41	99.37	99.35	99.37
	99.61	99.63	99.59	99.61	99.62	99.62
M-Net	96.21	96.11	96.39	96.25	96.28	96.27
	97.13	97.34	97.08	97.16	97.19	97.18
ResNet	95.63	95.02	95.93	95.72	95.75	95.74
	95.61	95.17	95.67	95.49	95.52	95.51
Eff.Net	96.13	96.01	96.37	96.21	96.23	96.22
	96.55	96.73	96.41	96.52	96.55	96.54
VGG-16	96.02	97.08	96.37	96.67	96.71	96.69
	96.99	97.13	96.69	96.71	95.94	95.97
VGG-19	97.72	97.59	97.47	97.35	97.37	97.34
	98.26	97.93	98.14	98.16	98.28	98.19
SAE	96.23	96.02	96.05	96.13	96.27	96.27
	96.78	96.55	96.32	96.21	96.15	96.16

authors used a normalization based imbalance handling, traditional generative techniques and a noise injection based approach. However, some of these studies did not regard the both the stability and adversarial robustness. Those that integrated noise injection did not emphasis the adaptive nature of injection which could control the extent of injected noise and maintain overall stability.

Secondly, our proposed Involution and Convolution based feature extraction scheme is the first of its kind within the domain of bearing fault classification. The proposed technique is chosen as feature extractor for its significant edge in effectively capturing spatial dependencies in a channel-agnostic manner, enabling it to recognize intricate patterns. Meanwhile, the complimentary Convolution is adept at detecting fundamental features and structures globally. The harmony of these two approaches achieves a more comprehensive understanding of the data and patterns compared to studies relying solely on convolutions or tedious hand-crafted details [20], [21], [22], [23], [24].

IV. CONCLUSION

In conclusion, this study introduced novel approach towards tackling critical issue of bearing fault detection. The vital importance of early detection in machinery to avoid expensive breakdowns and ensure operational safety cannot be overstated. The novel method proposed in this study combines Conditional Generative Adversarial Networks (CGANs) with spectral normalization and adaptive adversarial noise injection. The proposed method has demonstrated remarkable effectiveness in generating high-quality bearing fault samples. By reducing the risk of mode collapse and vanishing gradients, the proposed approach enhances the generalization and robustness of CGAN training, leading to more stable and reliable results.

Additionally, the first of its kind introduction of the I-C FFN feature extraction method, combining involution and convolution techniques for bearing fault classification, has further enriched the diagnostic capabilities by capturing both the local and global information, proving its versatility in handling various feature types, including channel-agnostic, spatial-specific, spatial-agnostic, and channel-specific characteristics. The gray-scaled converted bearing fault samples served as a perfect utility for channel agnostic and specific capabilities of our proposed involution-convolution synergy, yielding significant improvement in classification.

Our oversampling methodology has not only boosted the performance of the classification scheme but has also outperformed state-of-the-art transfer learning models, achieving impressive accuracy for both balanced and imbalanced schemes. The inclusion of the proposed oversampling method i.e., Adaptive Adversarial Class-Conditional GAN (AAC-cGAN) has significantly improved sample quality and robustness to noise, as demonstrated by various evaluation metrics employed in this study.

In the future, further research can explore the applicability of this approach in other domains beyond bearing fault diagnosis, potentially revolutionizing imbalanced dataset challenges in various fields. Additionally, refining the AAC-cGAN and feature extraction techniques can continue to push the boundaries of accuracy and reliability in fault detection.

ACKNOWLEDGMENT

The authors acknowledge the support from the Deanship of Scientific Research, Najran University. Kingdom of Saudi Arabia, for funding this work under the Distinguished Research funding program grant code number (NU/DRP/SERC/12/8).

REFERENCES

[1] H. Wang, S. Li, L. Song, and L. Cui, "A novel convolutional neural network based fault recognition method via image fusion of multi-vibration-signals," *Comput. Ind.*, vol. 105, pp. 182–190, Feb. 2019.

[2] S. Guo, B. Zhang, T. Yang, D. Lyu, and W. Gao, "Multitask convolutional neural network with information fusion for bearing fault diagnosis and localization," *IEEE Trans. Ind. Electron.*, vol. 67, no. 9, pp. 8005–8015, Sep. 2020.

[3] R. Huang, Y. Liao, S. Zhang, and W. Li, "Deep decoupling convolutional neural network for intelligent compound fault diagnosis," *IEEE Access*, vol. 7, pp. 1848–1858, 2019.

[4] H. Qiao, T. Wang, P. Wang, L. Zhang, and M. Xu, "An adaptive weighted multiscale convolutional neural network for rotating machinery fault diagnosis under variable operating conditions," *IEEE Access*, vol. 7, pp. 118954–118964, 2019.

[5] X. Peng, B. Zhang, and D. Gao, "Research on fault diagnosis method of rolling bearing based on 2DCNN," in *Proc. Chin. Control Decis. Conf. (CCDC)*, Aug. 2020, pp. 693–697.

[6] L. Wen, X. Li, L. Gao, and Y. Zhang, "A new convolutional neural network-based data-driven fault diagnosis method," *IEEE Trans. Ind. Electron.*, vol. 65, no. 7, pp. 5990–5998, Jul. 2018.

[7] J. Li, Y. Liu, and Q. Li, "Intelligent fault diagnosis of rolling bearings under imbalanced data conditions using attention-based deep learning method," *Measurement*, vol. 189, Feb. 2022, Art. no. 110500.

[8] S. Reed, Z. Akata, and X. Yan, "Generative adversarial text to image synthesis," in *Proc. Int. Erence Mach. Learn.*, 2016, pp. 1060–1069.

[9] A. Radford, L. Metz, and S. Chintala, "Unsupervised representation learning with deep convolutional generative adversarial networks," 2015, *arXiv:1511.06434*.

[10] N. V. Chawla, K. W. Bowyer, L. O. Hall, and W. P. Kegelmeyer, "SMOTE: Synthetic minority over-sampling technique," *J. Artif. Intell. Res.*, vol. 16, pp. 321–357, Jun. 2002.

[11] H. Tang, S. Gao, L. Wang, X. Li, B. Li, and S. Pang, "A novel intelligent fault diagnosis method for rolling bearings based on Wasserstein generative adversarial network and convolutional neural network under unbalanced dataset," *Sensors*, vol. 21, no. 20, p. 6754, Oct. 2021.

[12] Z. Wang, J. Wang, and Y. Wang, "An intelligent diagnosis scheme based on generative adversarial learning deep neural networks and its application to planetary gearbox fault pattern recognition," *Neurocomputing*, vol. 310, pp. 213–222, Oct. 2018.

[13] W. Mao, Y. Liu, L. Ding, and Y. Li, "Imbalanced fault diagnosis of rolling bearing based on generative adversarial network: A comparative study," *IEEE Access*, vol. 7, pp. 9515–9530, 2019.

[14] Q. Xuan, Z. Chen, Y. Liu, H. Huang, G. Bao, and D. Zhang, "Multiview generative adversarial network and its application in pearl classification," *IEEE Trans. Ind. Electron.*, vol. 66, no. 10, pp. 8244–8252, Oct. 2019.

[15] Y.O. Lee, J. Jo, and J. Hwang, "Application of deep neural network and generative adversarial network to industrial maintenance: A case study of induction motor fault detection," in *Proc. IEEE Int. Conf. Big Data*, Jun. 2017, pp. 3248–3253.

[16] T. Han, C. Liu, W. Yang, and D. Jiang, "A novel adversarial learning framework in deep convolutional neural network for intelligent diagnosis of mechanical faults," *Knowl.-Based Syst.*, vol. 165, pp. 474–487, Feb. 2019.

[17] P. Akhenia, K. Bhavsar, J. Panchal, and V. Vakharia, "Fault severity classification of ball bearing using SinGAN and deep convolutional neural network," *Proc. Inst. Mech. Engineers, C, J. Mech. Eng. Sci.*, vol. 236, no. 7, pp. 3864–3877, Apr. 2022.

[18] Q. Tong, F. Lu, Z. Feng, Q. Wan, G. An, J. Cao, and T. Guo, "A novel method for fault diagnosis of bearings with small and imbalanced data based on generative adversarial networks," *Appl. Sci.*, vol. 12, no. 14, p. 7346, Jul. 2022.

[19] D. Li, J. Hu, C. Wang, X. Li, Q. She, L. Zhu, T. Zhang, and Q. Chen, "Involution: Inverting the inherence of convolution for visual recognition," 2021, *arXiv:2103.06255*.

[20] Y. Yoo, H. Jo, and S.-W. Ban, "Lite and efficient deep learning model for bearing fault diagnosis using the CWRU dataset," *Sensors*, vol. 23, no. 6, p. 3157, Mar. 2023, doi: 10.3390/s23063157.

[21] M. Kahr, G. Kovács, M. Loinig, and H. Brückl, "Condition monitoring of ball bearings based on machine learning with synthetically generated data," *Sensors*, vol. 22, no. 7, p. 2490, Mar. 2022, doi: 10.3390/s22072490.

[22] H. N. Monday, J. Li, G. U. Nneji, S. Nahar, M. A. Hossin, J. Jackson, and A. Oluwasanmi, "A wavelet convolutional capsule network with modified super resolution generative adversarial network for fault diagnosis and classification," *Complex Intell. Syst.*, vol. 8, no. 6, pp. 4831–4847, Dec. 2022, doi: 10.1007/s40747-022-00733-6.

[23] S. Ayas and M. S. Ayas, "A novel bearing fault diagnosis method using deep residual learning network," *Multimedia Tools Appl.*, vol. 81, no. 16, pp. 22407–22423, Jul. 2022, doi: 10.1007/s11042-021-11617-1.

[24] B. U. Deveci, M. Celtikoglu, O. Albayrak, P. Unal, and P. Kirci, "Transfer learning enabled bearing fault detection methods based on image representations of single-dimensional signals," *Inf. Syst. Frontiers*, Feb. 2023, doi: 10.1007/s10796-023-10371-z.

[25] G. Lundberg and A. Palmgren, "Dynamic capacity of rolling bearings," *J. Appl. Mech.*, vol. 16, no. 2, pp. 165–172, Jun. 1949, doi: 10.1115/1.4009930.

[26] C. Wagner, A. Krinner, T. Thümmel, and D. Rixen, "Full dynamic ball bearing model with elastic outer ring for high speed applications," *Lubricants*, vol. 5, no. 2, p. 17, Jun. 2017, doi: 10.3390/LUBRICANTS5020017.

[27] *Balls and Ball Bearings for Medical Applications*. Accessed: Jul. 9, 2023. [Online]. Available: https://resources.hartfordtechnologies.com/blog/medical-applications-for-balls

[28] S. P. Lee, B. C. Kim, I. H. Lee, Y. G. Cho, and Y. C. Kim, "Distortion analysis for outer ring of automotive wheel bearing," *Trans. Korean Soc. Mech. Eng. A*, vol. 36, no. 12, pp. 1613–1618, Dec. 2012, doi: 10.3795/ksme-a.2012.36.12.1613.

[29] T. Plazenet, T. Boileau, C. Caironi, and B. Nahid-Mobarakeh, "A comprehensive study on shaft voltages and bearing currents in rotating machines," *IEEE Trans. Ind. Appl.*, vol. 54, no. 4, pp. 3749–3759, Jul. 2018, doi: 10.1109/TIA.2018.2818663.

[30] H. Tischmacher, "Bearing wear condition identification on converter-fed motors," in *Proc. Int. Symp. Power Electron., Electr. Drives, Autom. Motion (SPEEDAM)*, Jun. 2018, pp. 19–25, doi: 10.1109/SPEEDAM.2018.8445293.

[31] S. Kumar and S. Sen, "Wear and friction in journal bearing: A review," Tech. Rep., 2014.

[32] *Types of Bearing Classifications and How They Work*. Accessed: Jul. 8, 2023. [Online]. Available: https://www.thomasnet.com/articles/machinery-tools-supplies/bearing-types/

[33] *Types of Bearings | Uses and Working Mechanisms Explained*. Accessed: Jul. 8, 2023. [Online]. Available: https://fractory.com/types-of-bearings/

[34] H. Cheng, Y. Zhang, W. Lu, and Z. Yang, "Research on ball bearing model based on local defects," *Social Netw. Appl. Sci.*, vol. 1, no. 10, pp. 1–10, Oct. 2019, doi: 10.1007/S42452-019-1251-4.

[35] A. Gonda, R. Capan, D. Bechev, and B. Sauer, "The influence of lubricant conductivity on bearing currents in the case of rolling bearing greases," *Lubricants*, vol. 7, no. 12, p. 108, Dec. 2019, doi: 10.3390/LUBRICANTS7120108.

[36] J. Huan, S. Li, Z. Xia, Y. Wang, W. Wang, and G. Shi, "Experimental study on electric corrosion damage of bearing and solution," *Proc. Inst. Mech. Engineers, C, J. Mech. Eng. Sci.*, vol. 236, no. 19, pp. 10349–10358, May 2022, doi: 10.1177/09544062221100328.

[37] J. W. Jin, K. W. Kang, and S. Lee, "Fatigue analysis for automotive wheel bearing flanges," *Int. J. Precis. Eng. Manuf.*, vol. 24, no. 4, pp. 621–628, Apr. 2023, doi: 10.1007/S12541-023-00773-Z.

[38] A. Romanenko, A. Muetze, and J. Ahola, "Effects of electrostatic discharges on bearing grease dielectric strength and composition," *IEEE Trans. Ind. Appl.*, vol. 52, no. 6, pp. 4835–4842, Nov. 2016, doi: 10.1109/TIA.2016.2596239.

[39] N. Tandon and A. Choudhury, "A review of vibration and acoustic measurement methods for the detection of defects in rolling element bearings," *Tribol. Int.*, vol. 32, no. 8, pp. 469–480, Aug. 1999, doi: 10.1016/s0301-679x(99)00077-8.

[40] T. Harris, *Rolling Bearing Analysis*. Hoboken, NJ, USA: Wiley, 2001.

[41] P. D. McFadden and J. D. Smith, "The vibration produced by multiple point defects in a rolling element bearing," *J. Sound Vib.*, vol. 98, no. 2, pp. 263–273, Jan. 1985, doi: 10.1016/0022-460x(85)90390-6.

[42] C. S. Sunnersjö, "Rolling bearing vibrations—The effects of geometrical imperfections and wear," *J. Sound Vibrat.*, vol. 98, no. 4, pp. 455–474, Feb. 1985, doi: 10.1016/0022-460x(85)90256-1.

[43] *What's the Difference Between Bearings? | Machine Design*. Accessed: Jul. 9, 2023. [Online]. Available: https://www.machinedesign.com/learning-resources/whats-the-difference-between/article/21831901/whats-the-difference-between-bearings

[44] D. S. Chaudhari and V. Kumar, "Review paper of wear on journal bearing," *Int. J. Res. Appl. Sci. Eng. Technol.*, vol. 11, no. 5, pp. 4826–4828, May 2023, doi: 10.22214/ijraset.2023.52800.

[45] E. Yadav and V. K. Chawla, "An explicit literature review on bearing materials and their defect detection techniques," *Mater. Today, Proc.*, vol. 50, pp. 1637–1643, 2022, doi: 10.1016/j.matpr.2021.09.132.

[46] A. Shrestha and A. Mahmood, "Review of deep learning algorithms and architectures," *IEEE Access*, vol. 7, pp. 53040–53065, 2019, doi: 10.1109/ACCESS.2019.2912200.

[47] H. Li and J. Ji, "Bearing fault diagnosis with a feature fusion method based on an ensemble convolutional neural network and deep neural network," *Sensors*, vol. 19, no. 9, p. 2034, Apr. 2019, doi: 10.3390/s19092034.

[48] J. Yan, J. Kan, and H. Luo, "Rolling bearing fault diagnosis based on Markov transition field and residual network," *Sensors*, vol. 22, no. 10, p. 3936, May 2022, doi: 10.3390/s22103936.
[49] X. Zhao, M. Ma, and F. Shao, "Bearing fault diagnosis method based on improved Siamese neural network with small sample," *J. Cloud Comput.*, vol. 11, no. 1, p. 79, Nov. 2022, doi: 10.1186/s13677-022-00350-1.
[50] L. Xiao, X. Yang, and X. Yang, "A graph neural network-based bearing fault detection method," *Sci. Rep.*, vol. 13, no. 1, p. 5286, Mar. 2023, doi: 10.1038/s41598-023-32369-y.
[51] G. Wu, X. Ji, G. Yang, Y. Jia, and C. Cao, "Signal-to-image: Rolling bearing fault diagnosis using ResNet family deep-learning models," *Processes*, vol. 11, no. 5, p. 1527, May 2023, doi: 10.3390/pr11051527.
[52] *Download a Data File | Case School of Engineering | Case Western Reserve University*. Accessed: Jul. 8, 2023. [Online]. Available: https://engineering.case.edu/bearingdatacenter/download-data-file
[53] N. Rusk, "Deep learning," *Nature Methods*, vol. 13, no. 1, p. 35, Dec. 2015, doi: 10.1038/NMETH.3707.
[54] M. M. Taye, "Theoretical understanding of convolutional neural network: Concepts, architectures, applications, future directions," *Computation*, vol. 11, no. 3, p. 52, Mar. 2023, doi: 10.3390/COMPUTATION11030052.
[55] B. Zhao, X. Zhang, H. Li, and Z. Yang, "Intelligent fault diagnosis of rolling bearings based on normalized CNN considering data imbalance and variable working conditions," *Knowl.-Based Syst.*, vol. 199, Jul. 2020, Art. no. 105971, doi: 10.1016/j.knosys.2020.105971.
[56] Z. Li, T. Zheng, Y. Wang, Z. Cao, Z. Guo, and H. Fu, "A novel method for imbalanced fault diagnosis of rotating machinery based on generative adversarial networks," *IEEE Trans. Instrum. Meas.*, vol. 70, pp. 1–17, 2021, doi: 10.1109/TIM.2020.3009343.
[57] C. Yang, Z. Qiao, R. Zhu, X. Xu, Z. Lai, and S. Zhou, "An intelligent fault diagnosis method enhanced by noise injection for machinery," *IEEE Trans. Instrum. Meas.*, p. 1, 2023, doi: 10.1109/tim.2023.3322488.

MUHAMMAD IRFAN received the Ph.D. degree in electrical and electronic engineering from Universiti Teknologi PETRONAS, Malaysia, in 2016. From October 2009 to October 2011, he had industry experience. Since January 2017, he has academic experience in teaching and research. Currently, he is an Associate Professor with the Electrical Engineering Department, Najran University, Saudi Arabia. He has authored more than 250 research articles in reputed journals, books, and conference proceedings (Google Scholar Citations 2700 and H-index of 23). His current research interests include automation and process control, energy efficiency, condition monitoring, vibration analysis, artificial intelligence, the Internet of Things (IoT), big data analytics, smart cities, and smart healthcare.

ZOHAIB MUSHTAQ received the B.Sc. degree from Islamia University, the M.S. degree from Government College University, Lahore, and the Ph.D. degree in electrical engineering from the National Taiwan University of Science and Technology, in 2020. He was an Assistant Professor with Riphah International University. He is currently an Assistant Professor of electrical engineering with the University of Sargodha, Sargodha, Pakistan. He has published research in IEEE and other reputable journals. His current research interests include neural networks, machine learning, deep learning, computer vision, and data science.

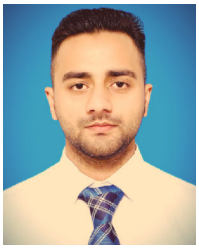

NABEEL AHMED KHAN received the Electrical Engineering degree from Riphah International University, Islamabad. His current research interests include deep learning, signal processing, computer vision, machine learning, and data science.

FAISAL ALTHOBIANI is currently an Associate Professor with the Marine Engineering Department, Faculty of Maritime, King Abdulaziz University, Jeddah, Saudi Arabia. He has more than six years of academic experience in teaching and research. He has authored several research papers in reputed journals, books, and conference proceedings. His current research interests include marine sciences, marine engineering, condition monitoring, and fault diagnosis systems.

SALIM NASAR FARAJ MURSAL received the Ph.D. degree in electronic and communication engineering. He has more than ten years of academic experience in teaching and research. He is currently an Assistant Professor with the College of Engineering, Najran University, Saudi Arabia. He has authored research papers in several journals, books, and conference proceedings.

SAIFUR RAHMAN received the Ph.D. degree in electrical and electronic engineering. He has more than 12 years of academic experience in teaching and research. Currently, he is an Associate Professor with the College of Engineering, Najran University, Saudi Arabia. He has authored more than 70 research papers in reputed journals, books, and conference proceedings. His current research interests include artificial intelligence, the Internet of Things (IoT), big data analytics, smart cities, and smart healthcare.

MUAWIA ABDELKAFI MAGZOUB (Member, IEEE) received the B.Sc. degree in electrical engineering from Al-Zaim Al-Azhari University, Khartoum, Sudan, in 2005, the master's degree in electronics engineering from the Sudan University of Science and Technology, Khartoum, in 2008, and the Ph.D. degree in electrical and electronics engineering from Universiti Teknologi PETRONAS, Malaysia, in 2017. He was a Lecturer with the Al-Jraif Sharq Technical College, Khartoum. He was a Senior Engineer with the Department of Tooling and Automation, Finisar II-VI (M) Sdn Bhd, Malaysia, for two years and eight months. He was a Postdoctoral Researcher with the Department of Electrical and Electronics Engineering, Universiti Teknologi PETRONAS, for one year. He is currently an Assistant Professor with the Department of Electrical and Electronics Engineering, Sudan Technological University, and National University, Sudan. His current research interests include automation and process control, power electronics, machine control and machine applications, artificial intelligence, smart grids, renewable energy and energy systems, machine learning, and data analysis.

MUHAMMAD ARMGHAN LATIF received the B.Sc. degree from the University of Management and Technology, Sialkot, Pakistan, and the M.S. degree from Cleveland State University, Cleveland, OH, USA. His current research interests include neural networks, machine learning, deep learning, computer vision, and data science.

IMRAN KHAN YOUSUFZAI received the B.Sc. degree in electrical engineering from the Federal Urdu University of Arts, Science and Technology, Islamabad, Pakistan, in 2010, the M.Sc. degree in control engineering from Mohammad Ali Jinnah University, Islamabad, in 2012, and the Ph.D. degree in control engineering from the Capital University of Science and Technology, Islamabad, in 2016. He has more than eight years of industrial and teaching experience. He was a Visiting Scholar with the Ohio State University, Columbus, USA. He is currently an Assistant Professor with the Department of Electrical Engineering, College of Engineering and Technology, University of Sargodha, Pakistan. His current research interests include the analysis and design of nonlinear control systems, especially sliding mode control, for various industrial applications.